Modification of vibrational selection rules in the photoinduced spin-crossover phase

Takeshi Tayagaki and Koichiro Tanaka

Department of Physics, Graduate School of Science, Kyoto University, Kyoto 606-8502, Japan

Hidekazu Okamura

Graduate School of Science and Technology, Kobe University, Kobe 657-8501, Japan

We show that vibrational selection rules are modified in the nonequilibrium photoinduced phase in the single-crystalline spin-crossover complex $[Fe(pic)_3]Cl_2EtOH$. In the Raman spectra, several infrared-active modes, forbidden by the selection rules in the thermally induced phase, appear in the photoinduced phase. In addition, these Raman lines are enhanced significantly as a result of resonant excitation to the intramolecular transition of the ligand molecule. These results indicate that the ligand molecule should be deformed drastically and the local symmetry breaks in the photoinduced phase.

I. INTRODUCTION

Phase-transition phenomena under external stimuli, such as heat, pressure, and magnetic field, have attracted much attention. Recently, it has been clarified that photoexcitation can stimulate a phase transition in several materials. These phenomena are called "photoinduced phase transition."[1−6] What is a unique characteristic of the photoinduced phase transition that differs from the other kinds of phase transitions, including thermally induced phase transition, has remained an unsolved problem.

The photoinduced phase transition has been attributed to the photoswitching phenomena to the macroscopic excited state. In the photoinduced phase transition, we can see several characteristics, such as threshold light intensity in the conversion efficiency and an incubation period in the initial stage of the temporal evolution.[4−6] These characteristics indicate that photoexcited states correlate with each other through a strong mutual correlation and form the macroscopic excited state. Such a correlation in photoinduced phase transition should be interesting and promise a development of material sciences.

The material properties and symmetry in the photoinduced phase have been quite similar to those in the thermally induced phase. For example, tetrathiafulvalene-chloranil takes an ionic phase as a *true* ground state, which is the lowest-energy state at the absolute zero. By increasing the temperature, the thermal excitation results in the thermally induced phase transition to the neutral phase.[7] The photoexcitation also stimulates the phase transition from the ionic phase to the photoinduced neutral phase, which has the same optical property and the crystal structure as those in the thermally induced phase.[4,8] As a result, the photoinduced phase transition has been implicitly considered as a switching phenomenon between a *true* ground state and the excited state by photoexcitation, in the same way as the thermally induced phase transition is triggered by thermal excitation.

Recently, it was confirmed that additional Raman lines, not observed in the thermally induced phase or the *true* ground state, appear in the photoinduced phase in a spin-crossover complex $[Fe(pic)_3]Cl_2EtOH$ (pic=2-picolylamine

=2-aminomethyl-pyridine, EtOH=ethanol).[9] As compared with the infrared-absorption spectra,[10] these Raman lines are infrared-active modes in the photoinduced phase. These results suggest that structural change should take place in the photoinduced phase transition leading to a different structure from the thermally induced phase or the *true* ground state.

The $3d^6$ electrons in the Fe^{2+} ion in $[Fe(pic)_3]Cl_2EtOH$ take two different spin states according to the strength of the ligand field splitting between t_{2g} and e_g orbitals: in the weak ligand field, the ground state takes a high-spin state $^5T_2$, while, in the strong field, it takes a low-spin state $^1A_1$. From the magnetic measurement at temperatures 300–4.2 K, Fe^{2+} ion takes a low-spin state at low temperatures, corresponding to the *true* ground state. As the temperature increases, a first-order phase transition takes place from the low-spin state to the high-spin state. In the thermally induced phase transition, entropy change including vibrational entropy, which could be estimated by Raman spectroscopy, plays an important role.[11] Such a phase transition takes place in two steps at the transition temperatures of 114 and 121 K.[12] The space group of the unit cell has been kept in monoclinic $P2_1/c$, $Z=4$ with the symmetry unchanged.[13]

Photoexcitation below about 50 K results in the photoinduced phase transition from the low-spin state to the high-spin state. The electronic transition (e.g., $^1A_1 \rightarrow ^1T_1$) is stimulated by the photoexcitation, and the excited electrons relax to induce a local lattice distortion via electron-lattice interaction (e.g., $^1T_1 \rightarrow ^3T_1 \rightarrow ^5T_2$).[14] In addition, the characteristics of the photoinduced phase transition, such as the thresholdlike behavior and incubation period, have been confirmed.[6] Such a photoinduced high-spin state goes back to the low-spin state in a finite lifetime dependent on the temperature. The photoinduced high-spin state has quite a long lifetime of about 10^4 sec at 10 K, but, at 50 K, it returns quickly within a few seconds.

In our previous experiments, the penetration depth of the photoexcitation for the photoinduced phase transition was quite short,[9] and the infrared-absorption spectra were measured in a powder sample.[10] Such spatially inhomogeneous photoexcitation might induce a disordered phase with stresses and strains. Whether the spectral change observed in

the previous experiment is caused by an intrinsic property of the crystal or by the inhomogeneity described above was impossible to determine. In addition, we have already proposed the Jahn-Teller distortion around the Fe^{2+} ion as a possible candidate for the structural change in the photoinduced high-spin state.[9] X-ray-absorption spectroscopy has clarified that the local structure around the Fe^{2+} ion in the photoinduced high-spin state should be quite similar to that in the high-temperature high-spin state.[15] There is, at a glance, a discrepancy between the results of the two experiments, which has remained an unsolved problem.

In this paper, we investigate Raman spectra and infrared-absorption spectra in the photoinduced phase that is generated by spatially homogeneous photoexcitation in a single crystal. In the Raman spectra, several infrared-active modes, not allowed by the selection rule in the thermally induced phase, appear in the photoinduced phase. The appearance indicates that the vibrational structures reflecting the local symmetry in the unit cell should be modified in the photoinduced phase. In addition, resonant Raman spectra with varying excitation energies have been examined in order to clarify the structural change in the photoinduced phase. These additional Raman lines are enhanced under resonant excitation into the intramolecular transition of the ligand molecule or picolylamine molecule. The strong resonant enhancement suggests that the local-symmetry breaking should take place in the ligand molecules. These results are consistent with the results of previous x-ray-absorption spectroscopy.

II. EXPERIMENT

$[Fe(pic)_3]Cl_2EtOH$ is synthesized from iron chloride dehydrate, 2-picolylamine, and ethanol under an O_2-free dry-nitrogen atmosphere. Single crystals of $[Fe(pic)_3]Cl_2EtOH$ are prepared by the evaporation method in a dry-nitrogen atmosphere. The typical size of the crystal is about $1 \times 1 \times 0.2$ mm³.

In Raman spectroscopy, a cw-neodymium vanadate (Nd:YVO₄) laser (1342 nm, 0.92 eV) is used as an excitation light source with an average power of 60 mW. The excitation laser is focused to a diameter of about 20 μm on the sample. The scattered light is collected in the backscattering geometry and dispersed by a single monochromator (Jobin Yvon, TRIAX-320, $f = 32$ cm) with a Raman notch filter (Super notch filter, Kaiser Op. Systems, Inc.). A 300-grooves/mm grating with a 1000 nm blaze is used. Raman signals are detected by a liquid-nitrogen-cooled indium-gallium-arsenide (InGaAs) array detector (Jobin Yvon, Spectrum One). The resolution of the experimental setup is 1.1 nm, corresponding to 6 cm⁻¹ at 1400 nm. The practical intensity of Raman signals is about 10 counts/sec. The typical integration time for measurement is about 300 sec. The samples are mounted in a liquid-He flow-type cryostat to measure the temperature dependence. The excitation light for the Raman spectra measurement simultaneously plays a role as an excitation light for the photoinduced spin-crossover transition below 40 K. We confirmed almost all Fe ions transform to a high-spin state within 5 min.
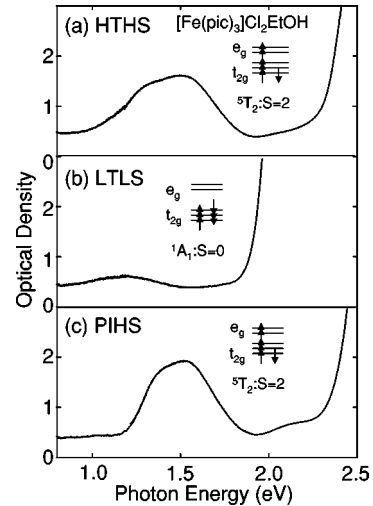

FIG. 1. Absorption spectra in the $[Fe(pic)_3]Cl_2EtOH$ single crystal measured at (a) 300 K, (b) 80 K, and (c) 10 K after the photoexcitation at 1.96 eV, corresponding to (a) the high-temperature high-spin state (HTHS), (b) low-temperature low-spin state (LTLS), and (c) photoinduced high-spin state (PIHS), respectively. The insets show the electron configurations of the ground state in these phases.

In the resonant Raman spectroscopy, a Ti:sapphire laser (1.56 eV), a helium-neon laser (1.96 eV), or second harmonics of a cw-neodymium vanadate (Nd:YVO₄) laser (2.33 eV) is used as an excitation light source. The scattered light is collected in the backscattering geometry and dispersed by a triple polychromator or a single monochromator with Raman notch filters. Raman signals are detected by a liquid-nitrogen-cooled charge-coupled-device detector.

The infrared-absorption spectra are measured using a synchrotron-radiation source and an infrared microscope at beam line BL43IR of SPring-8.[16] The infrared beam is focused to the area of about 20 μm in diameter on a thin crystal sample. To record the transmission spectra, a Fourier-transform interferometer and a HgCdTe photoconductive detector, with a resolution of 2 cm⁻¹, are used. The measurements are made at temperatures 290–10 K. A white light from a tungsten lamp is used for the photoexcitation of the photoinduced phase transition.

III. RESULTS

A. Absorption spectra

Figure 1 shows the absorption spectra in a $[Fe(pic)_3]Cl_2EtOH$ single crystal measured at (a) 300 K, (b) 80 K, and (c) 10 K after photoexcitation at 1.96 eV, corresponding to (a) the high-temperature high-spin, (b) low-temperature low-spin, and (c) photoinduced high-spin states, respectively. The insets show the electron configurations of the ground state. Based on the Tanabe-Sugano diagram,[17] the absorption band at 1.5 eV corresponds to the d-d transition from $^5T_2$ to ^1E in the high-temperature high-spin state. An absorption band above 2.3 eV is assigned to the intramolecular excitation of the ligand molecule. The absorption spectrum changes drastically at the thermally induced spin-
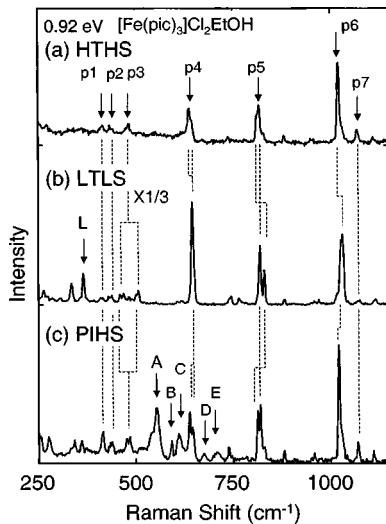
FIG. 2. Raman spectra of the $[Fe(pic)_3]Cl_2EtOH$ single crystal measured at (a) 190 K, (b) 100 K, and (c) 10 K, corresponding to (a) HTHS, (b) LTLS, and (c) PIHS, respectively. Labels $p1$–$p7$ show the vibrations of the ligand molecule. Labels A–E and L are described in the text.

crossover transition. The d-d transition shifts to a higher-energy side, resulting in an absorption band at 2.0 eV that corresponds to the transition from $^1A_1$ to $^1T_1$ in the low-temperature low-spin state. The weak absorption band around 1.2 eV is assigned to a spin-forbidden d-d transition from $^1A_1$ to $^3T_1$. In the present Raman study, we have used the 0.92 eV photoexcitation for the photoinduced phase transition, while, in the previous study, photoexcitation was at 2.33 eV.[9]

In Fig. 1(c), one can see that almost whole of the low-temperature low-spin state was transformed to the photoinduced high-spin state and not to a mixture of the low-temperature low-spin state and photoinduced high-spin state because the absorption band at 2.0 eV entirely disappears. The absorption spectrum in the photoinduced high-spin state is quite similar to that in the high-temperature high-spin state except for the band around 1.5 eV, the width of which in the photoinduced high-spin state becomes narrower than that in the high-temperature high-spin state. This width should result from the phonon sideband structure, reflecting the thermal distribution of the phonon structure. The difference between two states should be caused by the change of the temperature of the phonon system.

B. Raman spectra

Figure 2 shows the typical Raman spectra of the $[Fe(pic)_3]Cl_2EtOH$ single crystal in (a) the high-temperature high-spin state, (b) low-temperature low-spin state, and (c) photoinduced high-spin state measured at (a) 190 K, (b) 100 K, and (c) 10 K, respectively. We assigned the Raman lines, indicated by $p1$–$p7$ in Fig. 2(a), to the vibrational modes related to the ligand molecule by referring to the Raman spectrum of the picolylamine liquids, which is measured at room temperature. With lowering the temperature, several Raman lines change their intensities and positions at the ther-

mally induced phase transition ($T_C \sim 120$ K). We recognize the following Raman spectral changes: (i) Line L appears in the low-temperature low-spin state; (ii) the intensities of the lines $p3$, $p4$, $p5$, and $p6$ are enhanced by a factor of 3; (iii) line $p3$ splits into two peaks; (iv) lines $p4$, $p5$, and $p6$ shift to the higher-energy side. This result reflects the fact that the vibrational structure and electron-phonon interaction are modified at the thermally induced phase transition.

The excitation energy for the Raman spectroscopy corresponds to the spin-forbidden transition from $^1A_1$ to $^3T_1$ in the low-temperature low-spin state, and the excitation light for the Raman spectroscopy additionally results in the photoinduced phase transition below 40 K. Considering the small optical density at the excitation energy, only 15% energy of the excitation light is absorbed by the sample in the low-temperature low-spin state. The penetration depth of the laser at 0.92 eV is so long that the photoinduced phase transition can occur in a spatially homogeneous photoexcitation condition.

In the photoinduced high-spin state, several new lines that are hardly observed in the high-temperature high-spin and low-temperature low-spin states appear in the region from 500 to 750 cm^{-1}, as shown by arrows (e.g., line A). Lines $p1$-$p7$ are quite similar to those in the high-temperature high-spin state. Line L, appearing in the low-temperature low-spin state, almost disappears in the photoinduced high-spin state. The appearance of additional lines indicates that the photoinduced high-spin state has a crystal structure that differs from that in the high-temperature high-spin state. These results are essentially the same as those in our previous paper[9] and clarify the fact that the Raman spectral change in the photoinduced high-spin state should not be caused by distortion or stresses due to the short penetration depth.

The spectral change disappears quickly when the temperature is raised to above 50 K. In addition, no change is observed in the Raman spectrum with 1.56 eV laser excitation. This is because the reverse process from the photoinduced high-spin state to the low-temperature low-spin state by thermal excitation or light excitation[14] is predominant and the photoinduced high-spin state cannot be created as a result. It follows that the observed Raman spectral change should not come from the temperature-induced phase transition due to the heat effect by the photoexcitation but from an intrinsic and reproducible structural change in the photoinduced phase transition.

C. Temperature dependence of the Raman spectra

Figures 3(b)–3(d) show the temperature dependence of the integrated intensities of the Raman lines A, L, and $p6$. The high-spin fraction is also shown in Fig. 3(a). The intensity of line A is enhanced below 50 K, while it disappears abruptly above 50 K. Line A seems to have nonzero intensity above 120 K, which is not due to line A but to the background from the broad structure that differs from line A. It follows that line A is a Raman-active mode characterizing the photoinduced high-spin state. The intensity of line L is almost zero in the high-temperature high-spin state and in-
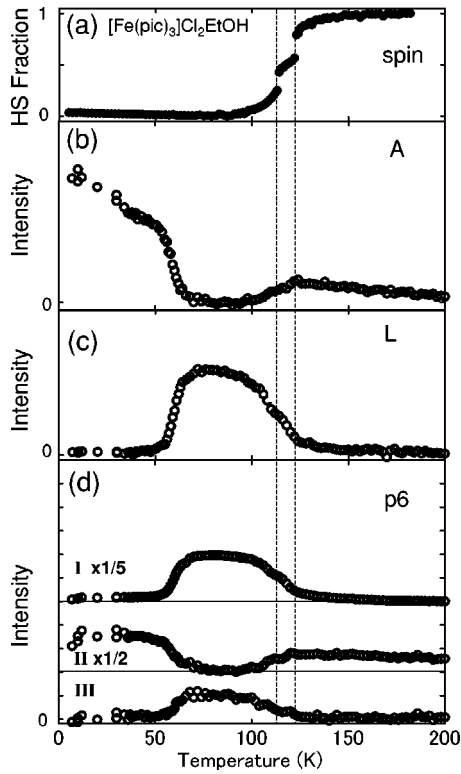
FIG. 3. Temperature dependence of (a) the high-spin fraction, and the intensities of Raman lines (b) A, (c) L, and (d) $p6$.

D. Resonant Raman spectra

Figure 4 shows the Raman spectra of the $[Fe(pic)_3]Cl_2EtOH$ single crystal measured by the 2.33 eV excitation at (a) 300 K, (b) 70 K, and (c) 30 K, corresponding to (a) the high-temperature high-spin, (b) low-temperature low-spin, and (c) photoinduced high-spin states. The excitation laser stimulates the d-d transition from $^1A_1$ to $^1T_1$ in the low-temperature low-spin state, leading to the photoinduced phase transition below 40 K. The additional Raman lines indicated by arrows appear only in the photoinduced high-spin state. Peak positions and relative intensities
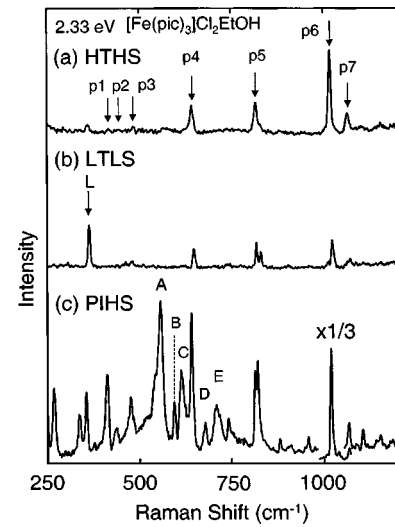

FIG. 4. Raman spectra of the $[Fe(pic)_3]Cl_2EtOH$ single crystal measured by the 2.33 eV excitation at (a) 300 K, (b) 70 K, and (c) 30 K, corresponding to (a) the HTHS, (b) LTLS, and (c) PIHS, respectively.

of these lines are identical to those measured by the excitation at 0.92 eV. In addition, the intensities of all Raman lines are enhanced significantly in the photoinduced high-spin state. The energy 2.33 eV corresponds to the absorption edge of the intramolecular transition of the ligand molecule in the photoinduced high-spin state. This result indicates that the magnitude of the electron-lattice interaction relating to the ligand molecule should be modified in the photoinduced high-spin state.

IV. DISCUSSION

A. Thermally induced spin-crossover transition

The two-step transition, as shown in Fig. 3(a), has been observed in the magnetic susceptibility at the thermally induced phase transition.[12] The intermediate phase between 114 K and 121 K has just one half of the susceptibility in the high-temperature high-spin state. Such an intermediate phase has been theoretically studied by using a two sublattice model[19] and Ising-like model including molecular vibrations,[20–22] in which the intermediate phase is an ordered mixed state of the high- and low-spin states. Although various experiments have been performed,[12,23] the mechanism of the two-step transition has not been experimentally clarified.

As shown in Figs. 3(b)–3(d), the thermally induced two-step transition can be observed in the Raman lines A, L, and $p6$. Line L should be related to the vibrational mode of Fe^{2+} because the enhancement of line L is observed by the excitation corresponding to the d-d transition (i.e., at 1.96 eV). Line $p6$ reflects the structural change of the ligand molecule. It follows that the local structure around the Fe^{2+} ion and the ligand molecule in the intermediate phase should be a mixture of those in the high-temperature high-spin and low-temperature low-spin states, as predicted by the theoretical study. In addition, line A, which is related to the photoinduced high-spin state, does not show any enhancement in the

creases abruptly around 120 K, synchronizing with the increase of the low-spin fraction. Line L disappears below 50 K. It follows that line L is a Raman-active mode characterizing the low-temperature low-spin state and that whole of the low-temperature low-spin state is converted to the photoinduced high-spin state below 50 K. Line $p6$ is assigned to the C-C ring stretching mode ν_1 of the pyridine ring in the ligand molecule.[18] Line $p6$ can be separated by three lines I–III. Line $p6$, which is a single line II in the high-temperature high-spin state, splits into two lines I, III in the low-temperature low-spin state. Lines I, III behave similarly to line L, while line II does opposite to line L. Coincident with a two-step transition observed in the high-spin fraction, the temperature dependence of lines A, L, and $p6$ reveals two kinks around the critical temperatures. It follows that the vibrational structure should strongly reflect the two-step spin transition.
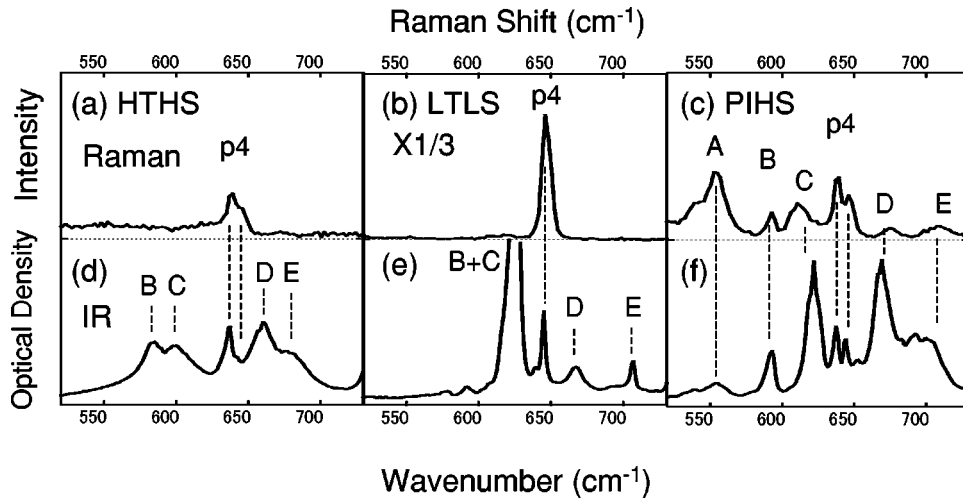
FIG. 5. Raman spectra measured at (a) 190 K, (b) 100 K, and (c) 10 K, corresponding to (a) the HTHS, (b) LTLS, and (c) PIHS, respectively. Infrared-absorption spectra measured at (d) 290 K, (e) 10 K, and (f) 10 K after photoexcitation by white light, corresponding to (d) the high-temperature high-spin state, (e) low-temperature low-spin state, and (f) photoinduced high-spin state, respectively. Labels A, B, C, D, E, and $p4$ are described in the text.

intermediate phase. It follows that the photoinduced high-spin state should be different from the intermediate phase.

B. Spectral change in the photoinduced phase

1. Comparison with the infrared absorption spectra

Figures 5(a)–5(c) show the Raman spectra in (a) the high-temperature high-spin state, (b) the low-temperature low-spin state, and (c) the photoinduced high-spin state. Figures 5(d)–5(f) show the infrared-absorption spectra from 500 to 750 cm^{-1} measured at (d) 290 K, (e) 10 K, and (f) 10 K after photoexcitation by white light, corresponding to (d) the high-temperature high-spin state, (e) the low-temperature low-spin state, and (f) the photoinduced high-spin state, respectively. Figure 5(c) shows that all parts of the crystal are transformed to the photoinduced high-spin state, and the fraction of the low-temperature low-spin state is less than 10%. The residual fraction would come from the reverse process to the low-temperature low-spin state by the white light irradiation. These infrared-absorption spectra measured on a crystal sample are essentially the same as those previously reported in the powder sample.[10,24] Table I summarizes the peak positions of the Raman-active and infrared-active lines in this region. In the infrared-absorption spectra, line A, suggesting a new vibrational structure, appears only in the photoinduced high-spin state.

In the high-temperature high-spin and low-temperature low-spin states, lines $B-E$ appear only in the infrared-absorption spectra. On the other hand, lines $B-E$ appear not only in the infrared-absorption spectrum, but also in the Raman spectrum in the photoinduced high-spin state. Peak positions of all these Raman lines, including line A, agree quite well with those of the infrared-absorption lines within the experimental error, as shown in Table I. All these results indicate that the Raman-active modes appearing in the photoinduced high-spin state originated from the infrared-active modes.

In the crystal with inversion symmetry, the Raman and infrared-absorption spectra have the complementary selection rule with each other: vibrational modes with even (odd) parity can be observed only in the Raman (infrared-absorption) spectra. Actually, the x-ray-diffraction measurement confirmed that the unit cells in the high-temperature high-spin and low-temperature low-spin states have a center of inversion symmetry,[25] which is consistent with our results. The violation of the selection rule in the photoinduced high-spin state suggests that the inversion symmetry should be broken in the photoinduced high-spin state.

2. Resonant Raman spectra

In order to clarify the structural change in the photoinduced high-spin state, it is essential to understand the origin

TABLE I. Peak positions in the Raman and the infrared-absorption (IR) spectra in the high-temperature high-spin state (HTHS), the low-temperature low-spin state (LTLS), and the photoinduced high-spin state (PIHS).

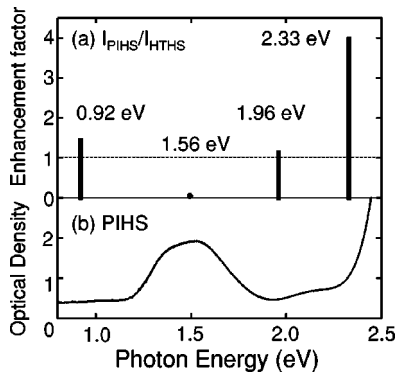| | HTHS | | LTLS | | PIHS | |
	Raman (cm^{-1})	IR (cm^{-1})	Raman (cm^{-1})	IR (cm^{-1})	Raman (cm^{-1})	IR (cm^{-1})
A					555	554
B		584		625	593	593
C		600		625	613	622
$p4$	639	637		639	639	637
	646	642	646	645	646	644
D		661		667	674	669
E		682		707	707	700

FIG. 6. (a) Enhancement factor in the Raman spectra measured by the excitation at 0.92 eV, 1.56 eV, 1.96 eV, and 2.33 eV. The intensities of Raman line $p6$ in PIHS are normalized from those in the HTHS. (b) Absorption spectrum in the photoinduced high-spin state.

of the lines $A-E$ characterizing the photoinduced high-spin state. Resonant Raman-scattering technique with tuning the excitation energy to an appropriate electronic transition is powerful for the assignment of Raman lines. We measured Raman spectra with the excitation at 0.92 eV, 1.56 eV, 1.96 eV, and 2.33 eV. Raman spectra measured by excitation at 0.92 eV and 1.96 eV are nonresonant in the photoinduced high-spin state because the energies 0.92 eV and 1.96 eV correspond to no absorption band. The energies 1.56 eV and 2.33 eV correspond to the d-d transition and the absorption edge of the intramolecular transition of the ligand molecule, respectively. The Raman spectroscopy with the 2.33 eV excitation corresponds to the preresonant Raman scattering to the intramolecular transition of the ligand molecule and reflects the electron-lattice interaction relating to the ligand molecule. The peak positions and relative intensities of the Raman lines in both the photoinduced high-spin and the high-temperature high-spin states are independent of the excitation energy, except for the excitation at 1.56 eV, which is unable to generate the photoinduced high-spin state.

Figure 6(a) shows the enhancement factor of the Raman intensity of the $p6$ line as a function of the excitation energy. The enhancement factor is defined as the intensity in the photoinduced high-spin state divided by that in the high-temperature high-spin state. The enhancement factor increases by a factor of about 4 for the excitation at 2.33 eV, while the intensities are almost unchanged between the photoinduced high-spin state and high-temperature high-spin state for the excitation at 0.92 eV and 1.96 eV. These results indicate that the electron-lattice interaction related to the ligand molecule should be modified in the photoinduced high-spin state. A similar resonance effect is confirmed for intensities of the additional Raman lines $A-E$ at the 2.33 eV excitation. This means that lines $A-E$ should also be assigned to the vibrational modes relating to the ligand molecule. Appearance of line A, which appears only in the photoinduced high-spin state, suggests that a structural deformation should take place in the ligand molecule, and the deformation should be strongly related to the violation of the vibrational selection rules in the photoinduced high-spin

state. A possible candidate for the new line A in the photo-induced high-spin state is an N-C-C bending mode in the amino-methyl base.

C. Unit-cell structure of the photoinduced high-spin state

As shown in the preceding section, the Raman and infrared-absorption spectra suggest that the inversion symmetry should be broken in the photoinduced high-spin state. Recently, x-ray-absorption spectroscopy[15] was made in the same system and led to a result contradicting this study at a first sight: the interatomic distance between the Fe^{2+} ion and the nearest-neighbor nitrogen atom is the same both in the high-temperature high-spin state and photoinduced high-spin state and in the the local symmetry around the Fe^{2+} ion (O_h) is unchanged.

Possible explanation for the symmetry breaking in the high-spin state is to start from three kinds of structures with different scales: an octahedral core structure composed of Fe^{2+} ion and six nitrogen atoms (hereafter, called FeN_6 octahedron); a unit-cell structure including four FeN_6 octahedron and ligand molecules; a domain including many unit cells with a long-range order. The domain with a long-range order will be discussed later.

In the thermally induced phase transition to the high-temperature high-spin state, the FeN_6 octahedron is expanded, keeping O_h local symmetry unchanged. The unit cell is also expanded with the space group unchanged. In the high-temperature high-spin state, the lattice constant becomes large with increasing the temperature.[13] On the other hand, in the photoinduced phase transition, it seems likely that the unit cell cannot be expanded as large as in the high-temperature high-spin state, because the thermal fluctuation resulting in the lattice expansion is small in the photoinduced high-spin state, while the FeN_6 octahedron becomes large with the same local symmetry as in the high-temperature high-spin state. Such a difference in the unit cell has already been confirmed in $[Fe(ptz)_6](BF_4)_2$,[26] where the lattice constant in the photoinduced high-spin state is much smaller than in the high-temperature high-spin state.

The expansion of the FeN_6 octahedron and the suppression of the unit-cell expansion should give rise to physical pressure to the ligand molecule, as illustrated in Fig. 7(a). As a result, the pressure induces the deformation of the ligand molecule, resulting in the symmetry breaking of inversion in the unit cell. One of the possible structural changes is a distortion of the carbon atom related to the N-C-C bending mode in the amino-methyl base, as illustrated in Fig. 7(b). In this case, the symmetry of the unit cell changes to $P1$, where the center of inversion symmetry disappears. In this way, the deformation of the ligand molecule leads to the violation of the selection rule, resulting in the appearance of infrared-active modes in the Raman spectrum in the photoinduced high-spin state. The deformation of the ligand molecule also modifies the electron-lattice interaction of the ligand molecule, which is consistent with the result that the Raman lines in the photoinduced high-spin state are enhanced in the resonant excitation to the intramolecular transition of the ligand molecule.
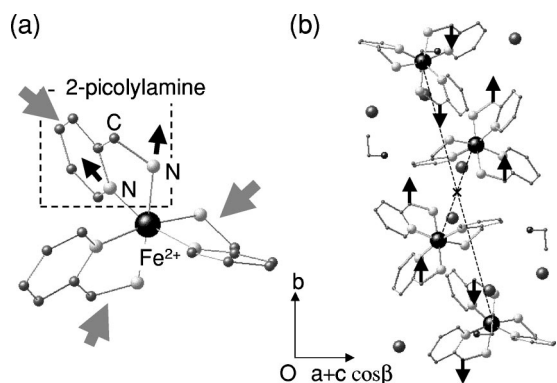
FIG. 7. (a) Local structure around Fe^{2+} ion in $[Fe(pic)_3]Cl_2 EtOH$. The arrows indicate a physical pressure to the ligand molecule. (b) Possible candidate of the distortion in the unit cell in the photoinduced high-spin state is indicated by the arrows.

The violation of the vibrational selections rule strongly suggests a local-symmetry breaking in the photoinduced high-spin state. However, the result does not mean directly that inversion symmetry is broken globally in a large domain including many unit cells as a single phase. In the extreme case, one can expect that deformations take place without a long-range order: Magnitudes and directions of the deformation may be distributed inhomogeneously in a site-to-site dependent manner, whereas the inversion symmetry with the long-range order may be kept in an average. In other words, a local-symmetry breaking should take place as a structural disorder in the crystal. The disorder may be the characteristic of the photoinduced phase transition as the nonequilibrium phase transition. Of course, one can also expect another possibility where the inversion-symmetry breaking takes place globally, that is, the structural change in the crystal takes place homogeneously in all unit cells. Unfortunately, we cannot determine which model is correct in this system only from the Raman, infrared-, or x-ray absorption spectroscopy, because these methods are relevant to only a local

structure. X-ray-diffraction measurements in the photoinduced high-spin state should be essential to clarify the long-range order.

V. CONCLUSION

We demonstrated that the photoinduced phase transition has unique characteristics that are different from those of the thermally induced phase transition. We have observed that several infrared-active modes, prohibited by the selection rule in the thermally induced phase, appear in the Raman spectrum of the photoinduced phase. From the resonant Raman spectra, modification of the vibrational selection rules should come from the deformation of the ligand molecule in the photoinduced phase. These results indicate that a vibrational structure with a local symmetry broken should be created by the photoinduced phase transition. X-ray-diffraction measurement in the photoinduced phase is in progress and soon become available to clarify whether the broken symmetry has a long-range order or not.

Note added in proof. The recent x-ray-diffraction experiments for the photoinduced high-spin state have shown the same space group with different lattice constants as the high-temperature high-spin state.[27] The result is not contradictory with the present results since the x-ray diffraction proves the long-range order in an average structure.

[1] *Relaxation of Excited States and Photo-Induced Structural Phase Transitions*, edited by K. Nasu (Springer, Berlin, 1997).

[2] K. Nasu, H. Ping, and H. Mizouchi, J. Phys.: Condens. Matter **13**, R693 (2001).

[3] S. Koshihara, Y. Tokura, K. Takeda, and T. Koda, Phys. Rev. Lett. **68**, 1148 (1992).

[4] S. Koshihara, Y. Takahashi, H. Sakai, Y. Tokura, and T. Luty, J. Phys. Chem. B **103**, 2592 (1999).

[5] K. Miyano, T. Tanaka, Y. Tomioka, and Y. Tokura, Phys. Rev. Lett. **78**, 4257 (1997).

[6] Y. Ogawa, S. Koshihara, K. Koshino, T. Ogawa, C. Urano, and H. Takagi, Phys. Rev. Lett. **84**, 3181 (2000).

[7] J.B. Torrance, J.E. Vazquez, J.J. Mayerle, and V.Y. Lee, Phys. Rev. Lett. **46**, 253 (1981).

[8] E. Collet, M. Lemée-Cailleau, M. Cointe, H. Cailleau, M. Wulff, T. Luty, S. Koshihara, L. Toupet, P. Rabiller, and S. Techert, Science **300**, 612 (2003).

[9] T. Tayagaki and K. Tanaka, Phys. Rev. Lett. **86**, 2886 (2001).

[10] T. Tayagaki and K. Tanaka, J. Lumin. **94-95**, 537 (2001).

[11] A. Bousseksou, J. McGarvey, F. Varret, J. Real, J. Tuchagues, A. Dennis, and M. Boillot, Chem. Phys. Lett. **318**, 409 (2000).

[12] P. Gütlich, A. Hauser, and H. Spiering, Angew. Chem. **33**, 2024 (1994).

[13] M. Mikami, M. Konno, and Y. Saito, J. Acta Cryst. **36**, 275 (1980).

[14] A. Hauser, J. Chem. Phys. **94**, 2741 (1991).

[15] H. Oyanagi, T. Tayagaki, and K. Tanaka, in *X-Ray and Inner-Shell Processes*, edited by Augusto Marceli *et al.*, AIP Conf. Proc. No. 652 (AIP, Melville, NY, 2003), p. 438.

[16] H. Kimura, T. Moriwaki, S. Takahashi, H. Aoyagi, T. Matsushita, Y. Ishizawa, M. Masaki, S. Oishi, H. Ohkuma, T. Namba, M. Sakurai, S. Kimura, H. Okamura, H. Nakagawa, T. Takahashi, K. Fukui, K. Shinoda, Y. Kondoh, T. Sata, M. Okuno, M. Matsunami, R. Koyanagi, Y. Yoshimatsu, and T. Ishikawa, Nucl.

Instrum. Methods Phys. Res. A **467-468**, 441 (2001).

[17] Y. Tanabe and S. Sugano, J. Phys. Soc. Jpn. **9**, 753 (1954).

[18] A. Hynes and M. Venter, J. Chem. Phys. **93**, 7581 (1990).

[19] N. Sasaki and T. Kambara, Phys. Rev. B **40**, 2442 (1989).

[20] A. Bousseksou, J. Nasser, J. Linares, K. Boukheddaden, and F. Varret, J. Phys. I **2**, 1381 (1992).

[21] A. Bousseksou, F. Varret, and J. Nasser, J. Phys. I **3**, 1463 (1993).

[22] A. Bousseksou, H. Constant-Machado, and F. Varret, J. Phys. I **5**, 747 (1995).

[23] M. Sorai, J. Ensling, and P. Gütlich, Chem. Phys. **18**, 199 (1976).

[24] K. Tanaka and T. Tayagaki, Phase Transitions **75**, 689 (2002).

[25] From the x-ray-diffraction measurement (Ref. 13) the crystal structure is monoclinic $P2_1/c$, $Z=4$, and the unit cell is composed of four $[Fe(pic)_3]Cl_2EtOH$, as illustrated in Fig. 7(b). If the position of a $[Fe(pic)_3]Cl_2EtOH$ component is presented as (x,y,z), all atoms in a unit cell are described as (i) x, y, z, (ii) x, $1/2-y$, $1/2+z$, (iii) $-x$, $1/2+y$, $1/2-z$, and (iv) $-x$, $1-y$, $1-z$. The unit cell has several centers of inversion symmetry [i.e., (0 1/2 1/2)], as indicated by a cross in Fig. 7(b). The lattice constant decreases when the space group of the crystal remains unchanged at the thermally induced phase transition from the high-temperature high-spin state to the low-temperature low-spin state.

[26] J. Kusz, H. Spiering, and P. Gütlich, J. Appl. Crystallogr. **33**, 201 (2000).

[27] N. Huby, L. Guerin, E. Collet, L. Toupet, H. Cailleau, T. Tayagaki, and K. Tanaka, Phys. Rev. B **69**, 020101(R) (2004).